Nanoscale Advances

ROYAL SOCIETY OF CHEMISTRY

PAPER

View Article Online
View Journal | View Issue

Cite this: *Nanoscale Adv.*, 2025, **7**, 4480

RNA lipid nanoparticles stabilized during nebulization through excipient selection†

Kai V. Slaughter, ‡[ab] Daniela Isaacs-Bernal, ‡[bc] Eric N. Donders, [abc] Siming Wang, [bc] Sami G. Sabbah, [ab] Xiang (Olivia) Li, [bc] Mickael Dang, [bc] Isaac M. Jackiw, [de] Karen Y. T. Chan, [f] Pieter Cullis [f] and Molly S. Shoichet *[abcg]

Nebulization of lipid nanoparticles (LNPs) has demonstrated great potential for the treatment of various pulmonary disorders *via* therapeutic RNA delivery. However, during the nebulization process, LNPs are subjected to high shear forces that result in particle destabilization and consequent loss of cargo. Here, we provide a generalizable approach to stabilize LNPs by adjusting the nebulization buffer composition. We investigated the effect of buffer composition on nanoparticle size, RNA encapsulation efficiency, and LNP material recovery. We found that pH 5.0 citrate buffer reduces the loss of encapsulated RNA, poloxamer 188 maintains nanoparticle size and improves recovery, and glucose is important for an iso-osmotic solution. RNA encapsulated in nebulized LNPs maintained bioactivity as demonstrated with cellular uptake and functional siRNA delivery to Vero cells expressing nano luciferase. Together, this work shows a versatile strategy for the delivery of inhalable LNP-based RNA therapies.

Received 12th December 2024
Accepted 21st May 2025

DOI: 10.1039/d4na01034e

rsc.li/nanoscale-advances

1. Introduction

Delivery of RNA therapeutics to the lungs holds promise in treating pulmonary disorders. For example, viral infections can be treated by targeted degradation with RNA interference (RNAi),[1] and genetic diseases by restoring functional protein expression through the delivery of mRNA[2] or gene editing cargoes.[3] Clinically used lipid nanoparticle (LNP) formulations for RNA delivery that are administered intravenously predominantly accumulate in the liver.[4] Although LNP formulations have been developed to specifically target the lung following intravenous administration,[5,6] only a limited fraction reach the lung epithelium.[7–9] These targeting strategies often employ cationic lipids which can induce blood clotting.[10] To overcome the limitations of intravenously administered LNP delivery to the lungs, aerosolized formulations for topical pulmonary delivery *via* inhalation have been pursued.[11,12]

Nebulization produces a fine mist that, upon inhalation, can non-invasively deliver therapeutics deep into the lungs;[13] however, shear forces, generated by nebulization, can result in nanoparticle destabilization and reduced delivery efficacy.[14] Modifications to the LNP composition can improve particle stability following nebulization;[11,14] yet, these modifications may negatively impact potency. For example, increased PEG density was shown to improve LNP stability during nebulization,[11] but reduces cellular uptake.[15] Additionally, modifications to LNP compositions to allow mucosal penetration[16] and reduce interaction with lung surfactants[9] may negatively impact particle stability during nebulization. Therefore, a lipid composition-agnostic approach to stabilize LNPs during nebulization would be beneficial.

Maintaining the electrostatic complexation between cationic ionizable lipid amines and anionic RNA backbone phosphates[17] by reducing buffer pH can prevent loss of encapsulated RNA.[12,18,19] Particle agglomeration during nebulization can also hinder efficacy of delivery. Notably, the diameter of LNPs is important for both mucosal penetration and endocytosis, where increased size can hinder diffusion[20] and clathrin-mediated uptake mechanisms.[21]

Here, we developed a generalizable strategy to stabilize LNPs during nebulization by adjusting the composition of the buffer (Fig. 1). We first formulated LNPs using the clinically approved

[a]*Institute of Biomedical Engineering, University of Toronto, 164 College Street, Toronto, Ontario M5S 3G9, Canada. E-mail: molly.shoichet@utoronto.ca*

[b]*Donnelly Centre, University of Toronto, 160 College Street, Toronto, Ontario M5S3E1, Canada*

[c]*Department of Chemical Engineering & Applied Chemistry, University of Toronto, 200 College Street, Toronto, Ontario M5S 3E5, Canada*

[d]*Department of Mechanical and Industrial Engineering, University of Toronto, 5 King's College Road, Toronto, Ontario M5S 3G8, Canada*

[e]*Department of Chemical and Materials Engineering, University of Alberta, 116 St. NW, Edmonton, Alberta T6G 1H9, Canada*

[f]*Department of Biochemistry and Molecular Biology, University of British Columbia, 2350 Health Sciences Mall, Vancouver, British Columbia V6T 1Z3, Canada*

[g]*Department of Chemistry, University of Toronto, 80 St. George Street, Toronto, Ontario M5S 3H6, Canada*

† Electronic supplementary information (ESI) available. See DOI: https://doi.org/10.1039/d4na01034e

‡ These authors contributed equally to this work.

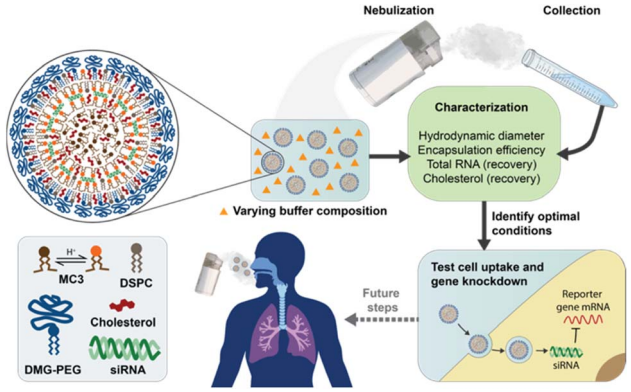

Fig. 1 Lipid nanoparticles (structure adapted from Kulkarni *et al.*[22]) were formulated with a series of nebulization buffers to determine the best stabilizing conditions. This lays the framework for future *in vivo* studies. Lung image was adapted from Sécher *et al.*[23] and collection tube image obtained from BioRender.com.

Onpattro® lipid composition and then assessed nebulization in different buffers in terms of hydrodynamic diameter, encapsulation efficiency, and nanoparticle material recovery. We demonstrated that a modified buffer formulation effectively stabilized multiple LNP formulations, highlighting its broad applicability. Finally, we confirmed that siRNA encapsulated in LNPs remained bioactive following nebulization in our selected buffer conditions.

2. Materials and methods

2.1 Materials

Cholesterol and sodium acetate were purchased from Sigma-Aldrich (St. Louis, MO). Ethanol and glacial acetic acid were purchased from Caledon Laboratories (Georgetown, ON, Canada). Phosphate buffered saline (PBS), Hank's balanced salt solution (HBSS), fetal bovine serum (FBS), penicillin–streptomycin, and trypsin–EDTA were purchased from Wisent Bioproducts (St. Bruno, QC, Canada). Distearoylphosphatidylcholine (DSPC), 1,2-dimyristoyl-*rac-glycero*-3-methoxypolyethylene glycol-2000 (DMG-PEG-2000), and dilinoleylmethyl-4-dimethylaminobutyrate (MC3) were purchased from Avanti Polar Lipids (Alabaster, AB). MC3 in Pieter Cullis' lab was synthesized by Dr Marco Ciufolini's group. 1,1′-Dioctadecyl-3,3,3′,3′-tetramethylindodicarbocyanine, 4-chlorobenzenesulfonate salt (DiD), EMEM, Quant-it™ RiboGreen RNA Assay Kit, and PrestoBlue HS Cell Viability Reagent were purchased from Thermo Fisher Scientific (Waltham, MA). Hoechst 33342 was purchased from Cell Signaling Technology (Danvers, MA). siRNAs were purchased from Integrated DNA Technologies (Coralville, IA).

2.2. Methods

2.2.1. LNP formulation. LNPs were formulated by combining siRNA (sequences in Table S1†) in acetate buffer (25 mM, pH 4.0) or mRNA (EZ Cap Firefly Luciferase mRNA (5-moUTP), ApexBio) in citrate buffer (50 mM, pH 4.0) with lipids in ethanol *via* a NanoAssemblr Benchtop microfluidic mixer (Precision Nanosystems, formulations 1 and 5–7) or a T-junction mixer (Cullis lab, formulations 2–4). The ethanol solution contained a lipid mix with 5.5 mM (formulations 1 and 5) or 10 mM (formulations 2–4) total lipid comprised of MC3 or SM-102, DSPC, cholesterol, DMG-PEG-2000 and DiD at a 50 : 10 : 38.5 : 1.5 : 0.1 molar ratio (unless otherwise specified). The aqueous and organic phases were mixed for a final ratio of ionizable lipid amines (N) to siRNA phosphate (P) of N/P = 3 or 6 for siRNA and N/P = 6 for mRNA. The resultant formulation was buffer exchanged to phosphate buffered saline and re-concentrated using Amicon Ultra-4 centrifugal filters (10 kDa MWCO). Formulations 2–4 were sterilized using a 200 nm filter prior to centrifugal filtration. LNP size and RNA encapsulation efficiency were characterized prior to dilution in nebulization buffer. LNPs were stored at 4 °C prior to conducting nebulization experiments. All LNP formulations used are listed in Table S2.†

2.2.2. Nebulization. LNPs were diluted in different nebulization buffers (Table S3†) to a target concentration of 300 nM of siRNA. Each formulation (1.5 mL) was nebulized *via* an Omron Mesh Nebulizer NE-U100 and collected in Eppendorf tubes attached to the nebulizer outlet. Particle size, cholesterol concentration, and siRNA quantification were evaluated in pre- and post-nebulized samples.

2.2.3. Dynamic light scattering (DLS). Hydrodynamic diameter (z-average) was measured using a DynaPro Plate Reader II (Wyatt Technologies) DLS instrument with a 60 mW, 830 nm laser and a detector angle of 158°. For initial post-formulation particle characterization, a 5 μL aliquot of each formulation was added into a 96-well plate and diluted with PBS to a final volume of 100 μL. Formulations in nebulization buffers before and after nebulization were measured undiluted (at 300 nM in terms of siRNA) in 100 μL. Hydrodynamic diameters were corrected according to solution viscosities. Measurements were obtained at 25 °C with 20 acquisitions per sample. Hydrodynamic diameter measurements of SM-102 LNPs were performed using a Malvern Nano-ZS instrument (Malvern Panalytical, Malvern, UK) equipped with a 4 mW, 632.8 nm laser and detector angle of 175°. For initial particle characterization, 25 μL of each formulation was diluted with PBS to a final volume of 1 mL. Formulations in nebulization buffers before and after nebulization were analyzed following a 2-fold dilution in the respective buffer to a final volume of 500 μL. Measurements were obtained at 25 °C with each sample undergoing 12 acquisitions per run measured in duplicate.

2.2.4. Cholesterol recovery measurement. Cholesterol concentration was determined using a Cholesterol E Total-Cholesterol assay (Wako Diagnostics, Richmond, VA) and a previously described protocol.[24] Briefly, LNPs in buffers before and after nebulization or cholesterol standards in ethanol were diluted 2-fold with cholesterol E reagent and incubated for 25 min at 37 °C before measuring absorbance at 595 nm using a Tecan Infinite Pro 200 plate reader. Cholesterol recovery was calculated using eqn (1):

$$\text{Cholesterol recovery (\%)} = \left(\frac{[\text{cholesterol}]_{\text{post-nebulization}}}{[\text{cholesterol}]_{\text{pre-nebulization}}}\right) \times 100\% \quad (1)$$

2.2.5. Quantification of RNA amount and encapsulation. Encapsulation efficiency and concentration of siRNA or mRNA was determined using a previously described Quant-iT RiboGreen assay.[24] Briefly, nanoparticle suspensions were diluted using Tris–EDTA (TE) buffer, either with (total RNA) or without (unencapsulated RNA) 1% Triton X-100. Stock LNP solutions were diluted 250-fold and LNPs in nebulization buffer were diluted 25-fold (except for SM-102 LNPs, which were diluted 2-fold) for a final volume of 100 μL in wells of a 96-well plate. Then, 100 μL of Quant-iT RiboGreen reagent was added to each well. Fluorescence intensity was measured using a Tecan Infinite Pro 200 plate reader. Encapsulation efficiency was calculated with eqn (2):

$$\text{Encapsulation efficiency (\%)} = \left(1 - \frac{\text{unencapsulated RNA}}{\text{total RNA}}\right) \times 100\% \quad (2)$$

Total and encapsulated RNA recovery was determined by measuring RNA concentrations before and after nebulization with the addition of 1% Triton X-100 and calculated using eqn (3) and (4), respectively:

$$\text{Total RNA recovery (\%)} = \left(\frac{[\text{RNA}]_{\text{free and encapsulated, post-nebulization}}}{[\text{RNA}]_{\text{free and encapsulated, pre-nebulization}}}\right) \times 100\% \quad (3)$$

$$\text{Encapsulated RNA recovery (\%)} = \left(\frac{[\text{RNA}]_{\text{encapsulated, post-nebulization}}}{[\text{RNA}]_{\text{free and encapsulated, pre-nebulization}}}\right) \times 100\% \quad (4)$$

2.2.6. Cell culture. Vero-E6-nLucP cells were a generous gift from Dr Roman Melnyk (Hospital for Sick Children). A humified incubator at 37 °C with 5% atmospheric CO_2 was used for cell maintenance. 75 cm^2 tissue culture flasks with 20 mL of EMEM media supplemented with 10% FBS, 10 UI/mL penicillin and 10 μg mL^{-1} streptomycin were used to culture cells. Passaging (with subculture ratios of 1 : 4 to 1 : 50 (v/v)) was performed once per week after detachment with trypsin–EDTA, pelleting cells by centrifugation, resuspension of cells in fresh media, and transfer into a new flask containing fresh media.

2.2.7. Cellular uptake. 2.5×10^3 Vero-nLucP cells suspended in 25 μL were added into each well of a 384-well plate (Greiner Bio-One 781079) and incubated overnight to allow adherence. 5 μL of diluted nanoparticle suspensions were dosed in triplicate. Then, 20 μL of complete cell growth media was added to ensure good mixing. Each well had a final siRNA concentration of 5 nM. After 3 h of incubation at 37 °C, the media was removed, and wells were washed with HBSS. Then cells were fixed with 4% (m/v) PFA in PBS for 15 min and stained with 5 μg mL^{-1} Hoechst in PBS for 15 min before fluorescence imaging as described below.

2.2.8. Wide-field fluorescence microscopy image acquisition. A Zeiss Apotome Live Cell System (Axio Observer Z.1 inverted fluorescence microscope) employing a long working distance 40× Plan Neofluor objective (NA = 0.6, Carl Zeiss Canada), X-Cite 120 LED fluorescence lamp (Lumen Dynamics), and an Axiocam 506 mono camera (Carl Zeiss Canada) was used to acquire fluorescence images. Images were autofocused based on the nuclei channel (Hoechst). For each well, four tiles were acquired and then stitched together as one image. Excitation and emission bands of 359–371 nm and >397 nm, respectively, were employed for Hoechst 33342. Excitation and emission bands of 625–655 nm and 665–715 nm, respectively, were employed for DiD. Exposure times of 200 ms for Hoechst 33342 and 500 ms for DiD were used with illumination at 100% laser power. These detector and illumination settings were constant for different wells and plates.

2.2.9. Image processing. MATLAB was used for image processing based on an algorithm originally created by Kameron Kilchrist.[25] The modified code can be accessed *via* GitHub (**https://github.com/kaislaughter/mChG8_image_processing**), and was used to identify and count cell nuclei (Hoechst 33342 stain) and endocytosed nanoparticles (DiD puncta), as described in our previous work.[26] Each biological replicate is the average of the results of three images from separate wells.

2.2.10. Model gene knockdown. 2×10^3 Vero-nLucP cells suspended in 100 μL were added to each well of a white-wall 96-well plate (Costar 3610) and incubated overnight to allow adherence. 20 μL of nanoparticles diluted in PBS to 20× the final concentration were dosed in triplicate. Then 80 μL of complete cell growth media was added to ensure good mixing. For each well, the final encapsulated siRNA concentration was 0.156–5.00 nM. The plate was incubated for 24 h at 37 °C and then treatments were removed. Total cellular metabolic activity was determined by adding PrestoBlue™ reagent in accordance with the manufacturer's instructions. After reading fluorescence, reagent was removed, and expression of nanoluciferase (nLuc) was quantified using the Nano-Glo® Luciferase Assay System. A Tecan Infinite Pro 200 plate reader was used to measure luminescence. Cell metabolic activity and nanoluciferase expression are plotted as a percentage, with normalization to cells treated with an equivalent volume of PBS. Reporter gene expression was normalized to cell metabolic activity. Non-linear regression was used to determine IC_{50} values using eqn (5):

$$\text{Normalized luminescence} = \frac{100\%}{1 + \left(\frac{[\text{siRNA}]}{IC_{50}}\right)} \quad (5)$$

Reported IC_{50} values were corrected by dividing by LNP recovery (in terms of total RNA) following nebulization.

2.2.11. Nebulized droplet diameter measurement. The diameters of the aerosolized droplets were measured using a Malvern Panalytical Spraytec, which uses a laser diffraction method to determine the volume-based droplet diameter distribution (Fig. S3a and b†). From the droplet diameter

distribution, the Spraytec calculates the median droplet diameter by volume, which is assumed to be equal to the MMAD in the present study as the sample densities are within 1% of the density of water. Sample densities were determined by measuring the mass of 1 mL of pipetted solution using a microbalance (Sartorius Cubis MSE125P 100-DI, Sartorius Lab Instruments GmbH & Co., Germany). The instrument was used with the 300 mm lens, providing a droplet size measurement range of 0.5–900 μm, and the software's automatic detector selection was used to minimize the effect of beam steering. The measurements were performed by activating and holding nebulizer under the path of the instrument's laser and approximately 15 cm from the detector array, as appropriate for the configuration, such that the aerosol plume passes through the path of the laser completely for the duration of the measurement. The instrument was operated in the rapid acquisition mode (2.5 kHz) and the data was averaged over a test duration of 5 seconds. Three samples of each solution were tested with two replicates of each sample. The replicate measurements were averaged to give the MMAD of each sample and the reported values of the MMAD (Fig. S3c†) are the average and standard deviation of the three samples of each solution.

3. Results and discussion

3.1 Nebulization buffer pH

We employed vibrating mesh nebulization as it has been shown to be a relatively gentle method for aerosolization of nanoparticle formulations[27] and is more commonly used than jet or ultrasonic nebulization for RNA delivery.[28] In particular, high shear stress from jet and ultrasonic nebulization can damage biomolecules.[29] Notwithstanding, even shear forces generated by vibrating mesh nebulization can destabilize LNPs.[14,30,31] To determine how best to minimize destabilization, we first investigated nebulization buffers with reduced pH to prevent loss of encapsulated RNA. Since high salt concentrations can reduce the strength of electrostatic complexes and screen repulsion between particles,[32,33] we began with saline-free buffer solutions.

LNPs were nebulized in 20 mM citrate (pH 4.0, 5.0 or 6.0) or 20 mM phosphate (pH 7.4) buffers. We found that pH had relatively minimal impact on particle size following nebulization, with substantial growth observed with all conditions tested, and the greatest increase at pH 7.4 (Fig. 2a). Polydispersity tended to increase post-nebulization, with a significant increase at pH 5.0 and 7.4, suggesting particle aggregation (Fig. S1a†). In contrast, pH significantly impacted the maintenance of siRNA encapsulation efficiency during nebulization, with a significant reduction at pH 6.0 and 7.4 *vs.* no or minimal change at pH 4.0 and 5.0 (Fig. 2b). We postulate that pH 4.0 and 5.0 buffers are sufficiently below the apparent pK_a of MC3 in the Onpattro® formulation (6.44)[34] and by remaining positively charged, MC3 could retain encapsulated siRNA if the particle integrity was compromised.

We measured the concentrations of: (1) siRNA before and after disruption of LNPs to determine encapsulated (eqn (4)) and total RNA recovery (eqn (3)); and (2) cholesterol as a proxy for lipid nanoparticle amount[35,36] pre- and post-nebulization to assess material recovery (eqn (1)). While siRNA encapsulation was improved at acidic pH, total RNA (Fig. 2c) and cholesterol (Fig. 2d) recovery after nebulization were low. Recovery of encapsulated RNA was low (~20%) at all pH values tested; thus, the increase in total RNA recovery at pH 7.4 was mostly due to free RNA. Total RNA recovery was negatively correlated with post-nebulization encapsulation efficiency, which may suggest that RNA lost from LNP disruption passed through the mesh

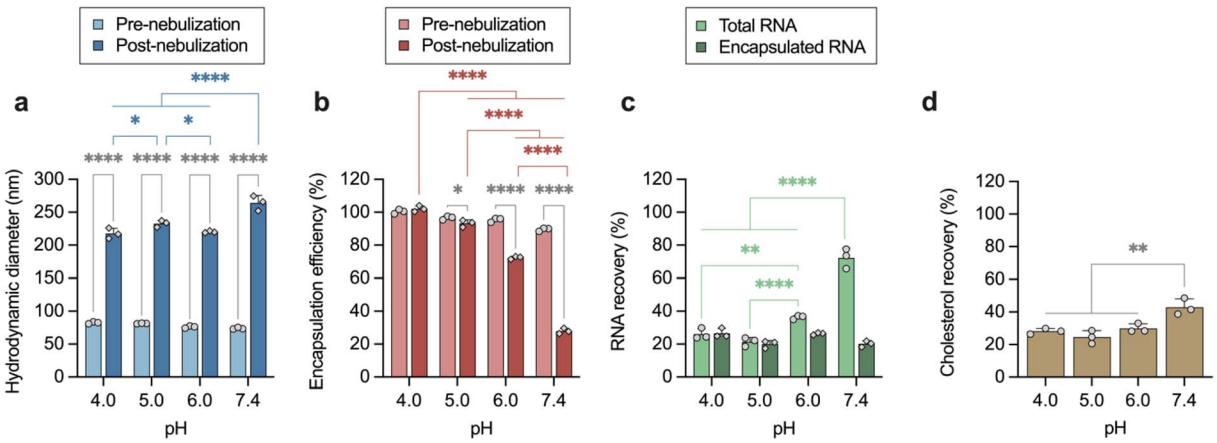

Fig. 2 Stabilization of LNPs depends on the nebulization buffer pH. Measurement of (a) hydrodynamic diameter, (b) encapsulation efficiency, (c) total and encapsulated RNA recovery and (d) cholesterol recovery for LNP nebulization in 20 mM citrate (pH 4.0, 5.0, or 6.0) or 20 mM phosphate (pH 7.4) buffers ((b) calculated as the unit difference of the ratio of unencapsulated siRNA and total siRNA expressed as a percentage. (c) and (d) calculated as the percentage ratio of post-nebulization and pre-nebulization concentration measurements, (a–c) – $n = 3$, ordinary two-way ANOVA, comparisons in gray made between pre-nebulization and post-nebulization conditions (Sidak's *post hoc* test), comparisons in blue or red made for post-nebulization conditions between each buffer (Tukey's *post hoc* test), comparisons in light green made between total RNA recovery measurements (Tukey's *post hoc* test), *$p < 0.05$, **$p < 0.01$, ****$p < 0.0001$, (d) – $n = 3$, mean ± standard deviation, ordinary one-way ANOVA with Tukey *post hoc* test, comparison made between all groups, **$p < 0.01$).

(Fig. S2†). However, low cholesterol recovery at all pH values tested indicates that most LNPs are likely entrapped in the mesh.

We hypothesized that nanoparticles aggregated during nebulization and got trapped in the mesh, accounting for the loss of RNA and cholesterol for intact particles. Furthermore, positively-charged particles (at pH values lower than the reported apparent pK_a of MC3 of 6.44) may have interacted with the nebulization mesh[37] to account for the reduction in cholesterol recovery for pH 4.0–6.0 buffers, compared to pH 7.4.

Notwithstanding the better recovery at pH 7.4, there was significantly greater post-nebulization RNA encapsulation at pH 4.0–6.0. We thus investigated strategies to maintain particle size and improve recovery following nebulization at low pH and specifically at pH 5.0, where siRNA encapsulation was only slightly reduced compared to pre-nebulized LNPs. We chose to work with the pH 5.0 (*vs.* pH 4.0) buffer to minimize potential toxicity associated with highly acidic inhaled solutions.[38] Previous studies have reported a lower bound of nebulization solution pH of 4.5,[39,40] with acidic solutions potentially resulting in airway irritation and bronchoconstriction.[41]

3.2 Addition of nonionic surfactants to nebulization buffer

To minimize size growth and improve particle recovery, we investigated the addition of two common nonionic surfactant types[42] in the nebulization buffer—polysorbates and poloxamers — as both have been shown to stabilize nanoparticles by sterically blocking aggregation.[43,44] LNPs were nebulized in 20 mM citrate buffer at pH 5.0 with the addition of 0.1% w/v of one of: polysorbate 20 (PS20), polysorbate 80 (PS80), poloxamer 188 (PX188) or poloxamer 407 (PX407). We found that PS80, PX188, and PX407 largely prevented particle aggregation after nebulization (Fig. 3a), with all surfactant-containing buffers resulting in a significantly lower post-nebulization size than without excipients. Surfactants PS20, PX188 and PX407 prevented an increase in polydispersity seen with no excipients or

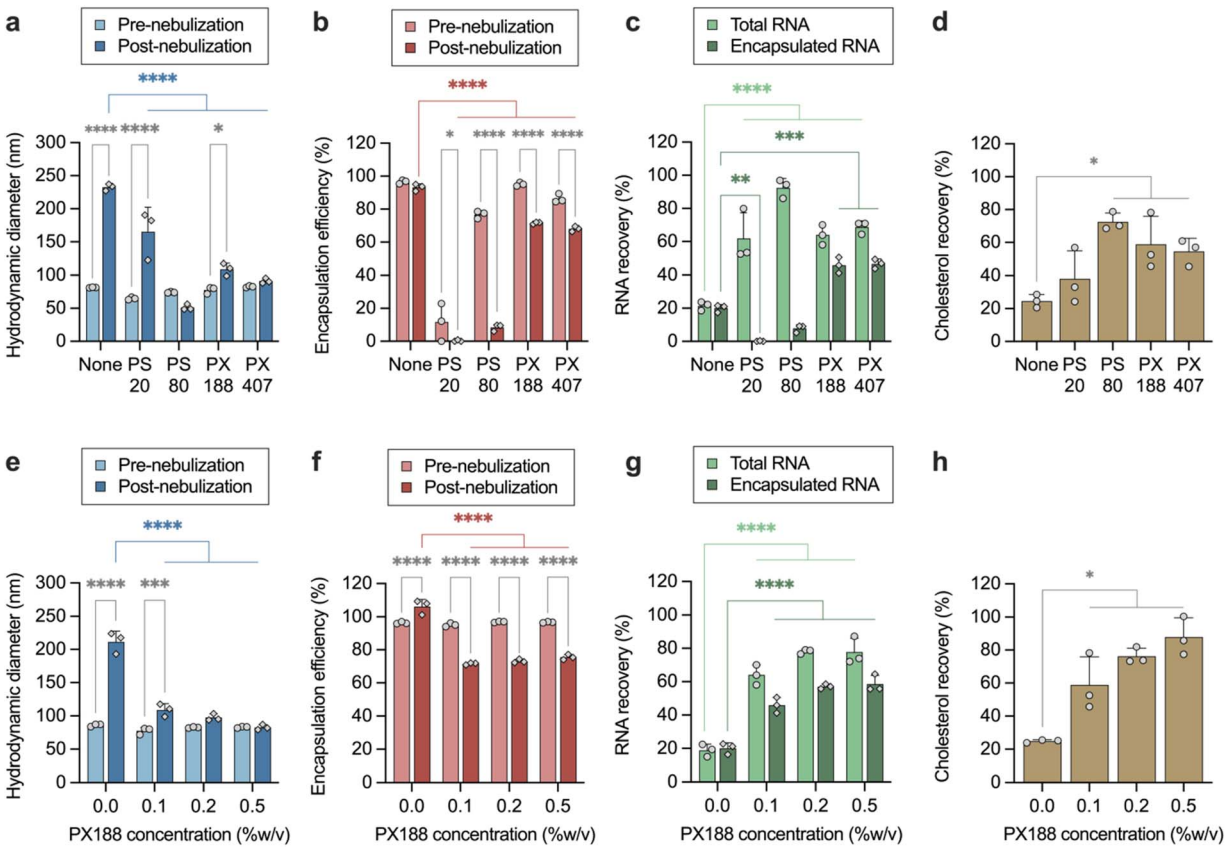

Fig. 3 Stabilization of LNPs during nebulization can be improved using surfactant polymer excipients. Measurement of (a) hydrodynamic diameter, (b) encapsulation efficiency, (c) total and encapsulated RNA recovery and (d) cholesterol recovery for LNP nebulization in 20 mM citrate buffer (pH 5) with varying surfactant polymers (0.1% w/v; values for "none" replotted from Fig. 2 for comparison). Measurement of (e) hydrodynamic diameter, (f) encapsulation efficiency, (g) total and encapsulated RNA recovery and (h) cholesterol recovery for LNP nebulization in 20 mM citrate buffer (pH 5) with varying concentrations of poloxamer 188 (PX188; values for 0.1% w/v replotted from panels (a)–(d)). ((a–c) and (e–g) $n = 3$, mean ± standard deviation, ordinary two-way ANOVA, comparisons in gray made between pre-nebulization and post-nebulization conditions (Sidak's *post hoc* test), comparisons in blue or red made for post-nebulization conditions between no excipients and each buffer (Dunnett's *post hoc* test), comparisons in light green made between total RNA recovery measurements and comparisons in dark green made between encapsulated RNA recovery measurements (Dunnett's *post hoc* test), *$p < 0.05$, **$p < 0.01$, ***$p < 0.001$, ****$p < 0.0001$, (d and h) $n = 3$, mean ± standard deviation, ordinary one-way ANOVA with Dunnett's *post hoc* test, comparison made between all groups and no excipient group, *$p < 0.05$).

PS80 (Fig. S1b†). However, all surfactant-containing buffers also resulted in reduced siRNA encapsulation after nebulization compared to surfactant-free buffers. Of the surfactants tested, poloxamers PX188 and PX407 resulted in maximal maintenance of siRNA encapsulation (Fig. 3b). PS20 resulted in siRNA leakage even before nebulization, which may be due to partial particle dissolution.

All of the non-ionic surfactants tested improved total RNA recovery, but only PX188 and PX407 improved encapsulated RNA recovery (Fig. 3c). PS80, PX188 and PX407 improved cholesterol recovery (Fig. 3d) after nebulization. Overall, PX188 and PX407 improved particle stability: siRNA encapsulation was maintained, and particle aggregation and material loss were limited in the nebulizer. Poloxamers may be better stabilizers than polysorbates due to their increased hydrophilic-lipophilic balance (HLB). A higher HLB (*i.e.*, longer hydrophilic chain) generally provides greater steric stabilization.[45] PX188 and PX407 have HLB values of 29 and 18–22, respectively, compared to HLB values of 16.7 and 15.6 for PS20 and PS80, respectively. Surfactants with HLB values of 15–18 have been used as solubilizers,[46] which likely explains the reduced encapsulation of siRNA with PS20 and PS80. We chose to use PX188 in further studies as it is less toxic than other surfactants in air–liquid interface culture.[47]

We investigated the effect of PX188 concentration (0.1, 0.2, and 0.5% w/v) on particle size, encapsulation efficiency, and total RNA and cholesterol recovery. All PX188 concentrations resulted in a significant reduction in post-nebulization size compared to a buffer without surfactant; however, only higher (0.2 or 0.5% w/v) PX188 concentrations resulted in no significant increase in size after nebulization (Fig. 3e). No significant increases in polydispersity index were observed for the three concentrations of PX188 tested (Fig. S1c†). All three concentrations similarly reduced siRNA encapsulation efficiency (Fig. 3f), yet improved recovery of both total and encapsulated RNA (Fig. 3g) and cholesterol (Fig. 3h). PX188 seemed to result in a concentration-dependent increase in nebulization time (data not shown); therefore, we utilized the lower 0.2% w/v PX188 in subsequent experiments, minimizing the amount of excipient needed to provide the desired stabilizing effect. While others have shown that branched PEG surfactants[12] or PX188 [18] in the nebulization buffer also reduced LNP size growth, we observed a more substantial effect: in these previous studies, LNPs grew in size by at least 50 nm in what were the best conditions compared to the non-significant change in size that we observed with our selected conditions. Similarly, another recent study using pH 6.0 HEPES buffer in combination with 8 mg mL^{-1} (0.8% w/v) PX188 reported about 20 nm in size growth post-nebulization.[19] We observed less growth with a lower concentration of PX188 in citrate buffer.

3.3 Iso-osmotic solutions for nebulization

Given the importance of iso-osmotic inhaled solutions for delivery to the lungs,[48] we investigated strategies to reach 300 mOsm L^{-1}. We tested iso-osmotic saline (0.9% w/v NaCl) and glucose (5% w/v), which have been used as nebulization media.[49,50] In the absence of PX188, particle size increased (Fig. 4a), polydispersity increased for NaCl but not for glucose (Fig. S1d†), siRNA encapsulation was largely maintained (Fig. 4b), and total and encapsulated RNA (Fig. 4c) and cholesterol (Fig. 4d) recovery were low for both iso-osmotic solutions. In contrast, nebulization in iso-osmotic solution with 0.2% PX188 largely prevented particle growth (with a significant reduction in post-nebulization size) or polydispersity increase, and improved total and encapsulated RNA and cholesterol recovery. In comparison to isotonic saline, use of iso-osmotic glucose resulted in no significant size growth, greater retention of encapsulated siRNA, and improved total and

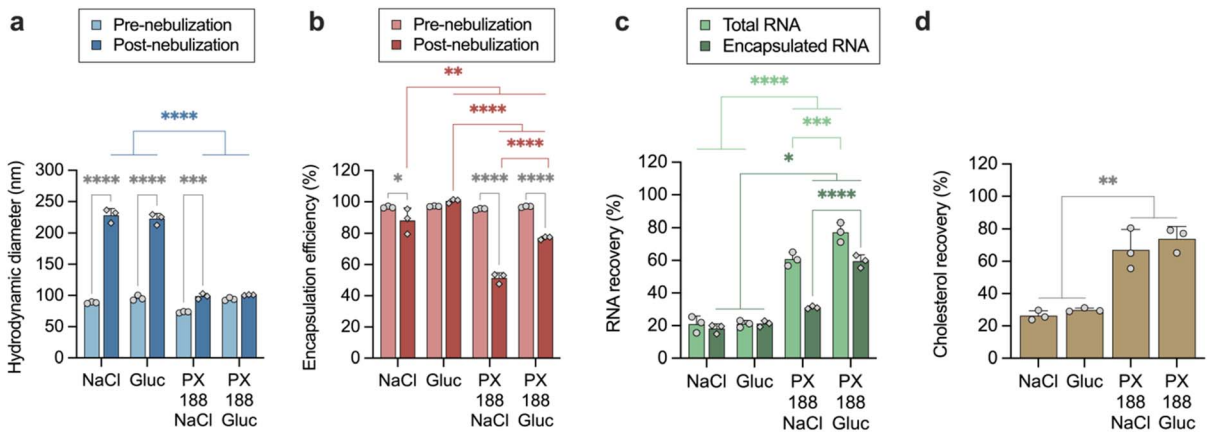

Fig. 4 Glucose is more suitable than sodium chloride for preparation of iso-osmotic solutions for LNP nebulization. Measurement of (a) hydrodynamic diameter, (b) encapsulation efficiency, (c) total and encapsulated RNA recovery, and (d) cholesterol recovery for LNP nebulization in 20 mM citrate buffer (pH 5.0) with varying iso-osmotic solutions (300 mOsm L^{-1} of sodium chloride (NaCl) or glucose (Gluc)). ((a–c) $n = 3$, mean ± standard deviation, ordinary two-way ANOVA, comparisons in gray made between pre-nebulization and post-nebulization conditions (Sidak's *post hoc* test), comparisons in blue or red made for post-nebulization conditions between each buffer (Tukey's *post hoc* test); comparisons in light green made between total RNA recovery measurements and comparisons in dark green made between encapsulated RNA recovery measurements (Tukey's *post hoc* test), *$p < 0.05$, **$p < 0.01$, ***$p < 0.001$, ****$p < 0.0001$, (d) $n = 3$, mean ± standard deviation, ordinary one-way ANOVA with Tukey post-hoc test, comparison between all groups, **$p < 0.01$).

encapsulated siRNA recovery. Increasing ion concentration through the addition of saline likely disrupted electrostatic complexes[32] between siRNA and the ionizable lipid (MC3) and screened electrostatic repulsion between nanoparticles whereas the addition of neutral glucose did not. In future applications where cold-storage or lyophilization may be required, glucose may act as a cryo-protectant or could be substituted for a more common LNP additive such as sucrose.[51]

3.4 Droplet size measurements for nebulized LNPs

Nebulized droplet size (mass median aerodynamic diameter; MMAD) is an important parameter in determining depth of lung deposition.[52] Based on our data, the best nebulization solution comprised 20 mM citrate, pH 5.0, with 0.2% w/v PX188 and 5% w/v glucose. We measured the MMAD of LNPs nebulized therein at 7.14 ± 0.14 μm, which is significantly smaller than those in 20 mM citrate buffer without PX188 of 7.54 ± 0.18 μm (Fig. S3†). Droplets with MMAD of 5–10 μm typically deposit in the oral pharynx and tracheobronchial tree, although distal lung regions may be accessed through particular breathing techniques.[53] Our MMAD measurements, conducted with laser diffraction, may have a larger size than others reported, due to possible droplet evaporation for longer detector pathlengths, such as with commonly used cascade impactors.[54] Future studies could employ a next generation impactor to estimate the lung deposition profile.[55]

3.5 Applicability to other LNP formulations

To determine whether our selected nebulization formulation was broadly applicable, we tested additional LNP formulations. First, LNPs prepared in another laboratory (with identical composition), when nebulized in our selected buffer, had minimal particle size growth, no significant increase in PDI, improved retention of encapsulated siRNA, and reduced loss of RNA and cholesterol relative to nebulization in PBS (Fig. S4a–e†). Second, we tested LNPs which were previously designed to improve circulation half-life through the incorporation of a high molar fraction (40 mol%) of egg sphingomyelin (ESM).[56] Two ESM-containing formulations were tested: one in which both MC3 and cholesterol were proportionally substituted with ESM (labelled ESM-A) and another where only MC3 was substituted with ESM (labelled ESM-B). As with the original LNPs tested, nebulization of both ESM-A (Fig. S4f–j†) and ESM-B (Fig. S4k–o†) in PBS resulted in particle disruption that was

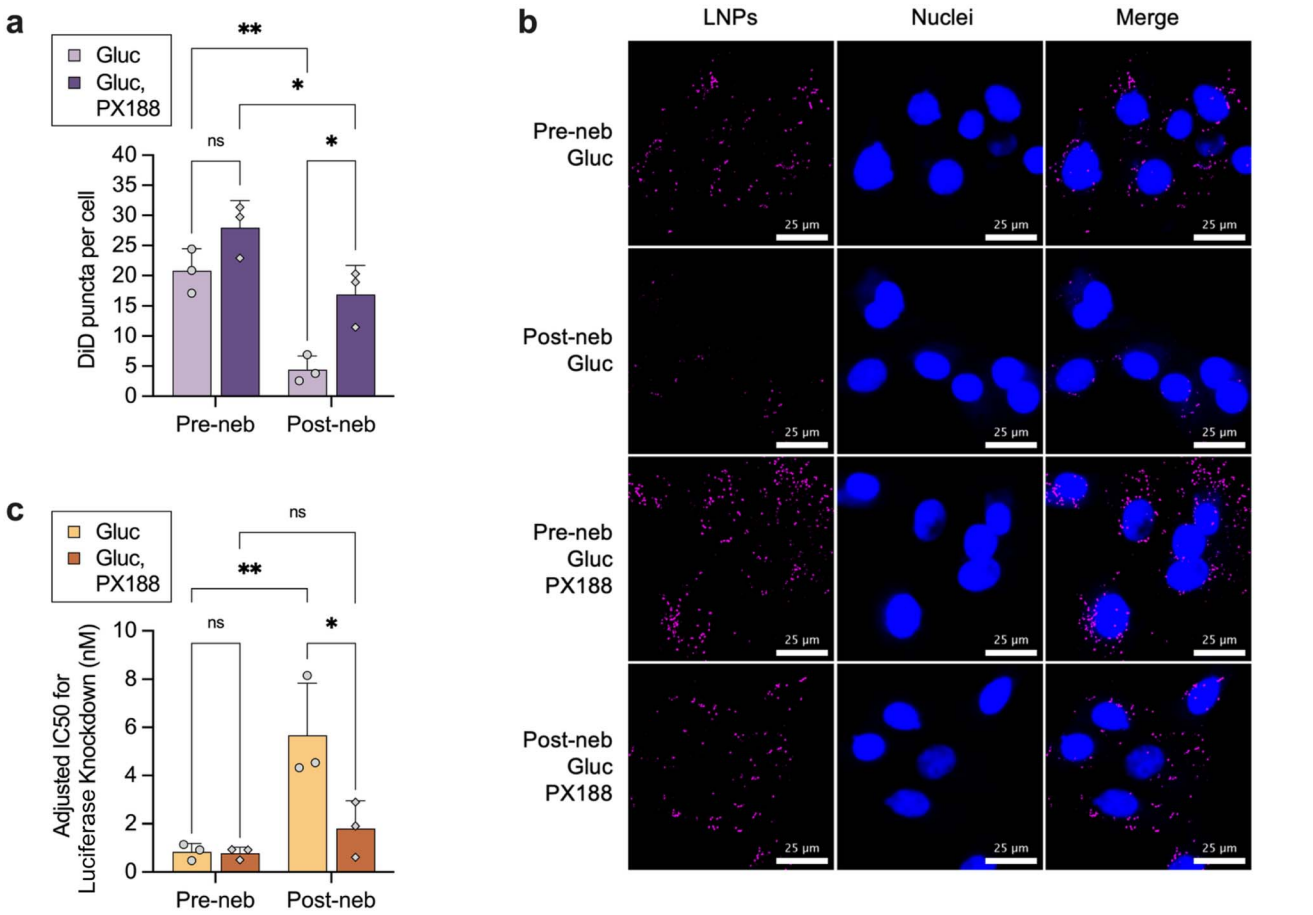

Fig. 5 LNPs nebulized in selected conditions retain biological activity. Measurement of (a) cellular uptake with (b) representative microscope images and (c) potency (recovery adjusted IC_{50}, described in methods) of nLuc knockdown in Vero cells for LNPs nebulized in citrate buffer with 5% glucose (Gluc) with or without 0.2% poloxamer 188 (PX188; $n = 3$, mean ± standard deviation, ordinary two-way ANOVA with Sidak's *post hoc* test, comparisons made between all groups (selected comparisons displayed) *$p < 0.05$, **$p < 0.01$, ns = not significant).

overcome by our selected formulation buffer of 20 mM citrate at pH 5.0 with 0.2% PX188 and 5% glucose. Interestingly, both ESM-containing formulations exhibited no significant post-nebulization reduction in encapsulation efficiency in these optimized conditions, unlike our trials with Onpattro®-like LNPs. This may be attributed to enhanced RNA protection conferred by the high phospholipid content, which has previously been shown to promote the formation of a solid lipid core within an aqueous compartment and enclosed by a bilayer.[56] We also demonstrated stabilization under these conditions using LNPs with the ionizable lipid, SM-102, which is used in the Moderna mRNA vaccine (Fig. S4p–t†). For all trials thus far, we used cholesterol recovery as a proxy for that of LNPs. We found that reduced cholesterol recovery correlated with increased LNP hydrodynamic diameter post-nebulization, supporting our hypothesis of LNP entrapment within the nebulizer mesh (Fig. S5†).

3.6 Bioactivity after nebulization in best conditions

We utilized Vero cells expressing nanoluciferase (nLuc) to test the efficacy of sinLuc *via* cellular uptake and reduction in luminescence. Since only about 20% of siRNA remained encapsulated after nebulization in 20 mM phosphate buffer at pH 7.4, we compared the efficacy of our improved buffer formulation (20 mM citrate, pH 5.0 with 0.2% PX188 and 5% glucose) with LNPs nebulized in 20 mM citrate buffer, pH 5.0, with 5% glucose. Glucose was included to adjust osmolarity, and thus only iso-osmotic formulations were evaluated in the bioactivity studies. First, we measured cellular uptake with nebulized LNPs labelled with a hydrophobic fluorescent 1,1′-dioctadecyl-3,3,3′,3′-tetramethylindodicarbocyanine, 4-chlorobenzenesulfonate salt (DiD) dye by fluorescence microscopy. We found significantly more nanoparticles in cells when LNPs were nebulized in an iso-osmotic citrate buffer at pH 5.0 with both glucose and PX188 *versus* without PX188 (Fig. 5a, representative images in Fig. 5b). Next, we measured nLuc knockdown to assess functional siRNA delivery using the same nebulization conditions and found greater potency with (*vs.* without) PX188 in the nebulization buffer (Fig. 5c, dose–response curve in Fig. S6a†). Knockdown IC_{50} values were normalized to RNA recovery (raw values in Fig. S6b†); thus, reduced potency is mainly attributed to material loss, with intact nebulized LNPs remaining similarly active.

To better understand the breadth of our selected stabilizing conditions, we tested LNPs encapsulating a model mRNA encoding firefly luciferase (mFLuc). As with siRNA-LNPs, we found that 20 mM citrate, pH 5.0 with 0.2% PX188 and 5% glucose stabilized mFLuc-LNPs during nebulization in terms of particle size (Fig. S7a†), polydispersity index (Fig. S7b;† although some increase occurred, it was less than conditions without PX188) encapsulated mRNA (Fig. S7c†) recovery of both total and encapsulated mRNA (Fig. S7d†), and cholesterol (Fig. S7e†). Nebulized mFLuc-LNPs delivered functional mRNA to Vero cells (with minimal impact on cell metabolic activity; Fig. S7f†), albeit with decreased potency relative to those before nebulization (Fig. S7g and h†). Others have also shown decreased mRNA activity following LNP nebulization,[31] which indicates that further optimization may be necessary. mRNA is more sensitive to environmental degradation than siRNA because double-stranded RNA is more stable than single-stranded RNA.[57]

4. Conclusions

We demonstrated stabilization of LNPs during nebulization by manipulating the formulation buffer. We found the best composition comprised 20 mM citrate, pH 5.0 with 0.2% PX188 and 5% glucose, which is broadly applicable to several LNP formulations. Low pH is likely only useful to stabilize electrostatic complexes with ionizable material; however, even LNPs formulated with permanent cationic lipids will likely be stabilized by PX188. Prevention of both aggregation as well as RNA and nanoparticle loss by nebulization with surfactant addition at low pH should be broadly useful for ionizable systems. Future studies could evaluate whether the stabilization strategies developed here are also applicable to other delivery systems, such as polymeric nanoparticles,[58] which are being investigated for pulmonary delivery. These stabilizing conditions could be evaluated with LNPs that are modified for enhanced mucous penetration and reduced lung surfactant interaction, which may improve efficacy *in vivo*. Recent studies have shown that LNPs employing DMG-PEG-2000 may induce anti-PEG antibodies, particularly with repeated administration, which could hinder treatment efficacy.[59–61] Future work could investigate our nebulization stabilization strategy with LNPs incorporating PEG alternatives such as zwitterionic polymers.[62] Interestingly, zwitterionic polymers have also been shown to improve LNP stability during nebulization.[63] Overall, this generalizable strategy for LNP stabilization during nebulization should be applicable to multiple RNA delivery strategies and may ultimately improve treatment of pulmonary disorders.

Data availability

The data supporting this article have been included in the manuscript and ESI† in the form of figures and tables. The raw data will be available upon request.

Author contributions

Conceptualization K. V. S. and D. I. B.; data curation K. V. S. and D. I. B.; formal analysis K. V. S. and D. I. B.; investigation K. V. S., D. I. B., E. N. D., S. W., S. G. S., X. L., M. D., I. M. J., and K. Y. T. C.; visualization K. V. S.; software K. V. S. and E. N. D.; methodology K. V. S. and D. I. B.; writing – original draft K. V. S., D. I. B and M. S. S.; writing – review & editing K. V. S., D. I. B., E. N. D., S. W., S. G. S., I. M. J., K. Y. T. C, M. S. S.; funding acquisition M. S. S.; resources P. C. and M. S. S.; supervision M. S. S.

Conflicts of interest

There are no conflicts to declare.

Acknowledgements

The authors thank J. Kulkarni, D. Witzigmann and other members of Professor Pieter Cullis' lab (UBC) for helpful discussions and providing LNP formulations. The authors thank L. Fiddes from the University of Toronto Microscope Imaging Laboratory for help with fluorescence imaging, R. Melnyk from the Hospital for Sick Children for providing Vero-nLucP cells, and members of the Shoichet lab for their thoughtful comments. This work was supported by the Natural Sciences and Engineering Research Council (NSERC Discovery RGPIN-2019-06933 and Herzberg GLDSU 537982-20 to M. S. S.). M. S. S. also acknowledges holding the Pamela & Paul Austin Chair in Precision & Regenerative Medicine. We are grateful for additional support to: K. V. S. from NSERC CGSM and CGSD, the Ontario Graduate Scholarship, the Barbara and Frank Milligan Graduate Fellowship, and the Cecil Yip Doctoral Research Award; D. I. B. from the NSERC CREATE in Programmed Molecules for Therapeutics, Sensing and Diagnostic (PROMOTE) Fellowship, the Delta Kappa Gamma World Fellowship, the Cecil Yip Doctoral Research Award, and the Precision Medicine Initiative (PRiME) Fellowship at the University of Toronto; E. N. D. from the Queen Elizabeth II Graduate Scholarships in Science & Technology, the Ontario Graduate Scholarship, and the Precision Medicine Initiative (PRiME) Fellowship (University of Toronto internal fellowship number PRMF2020-002). S. G. S. and S. W. were supported by NSERC Undergraduate Student Research Awards.

References

1 A. Idris, A. Davis, A. Supramaniam, D. Acharya, G. Kelly, Y. Tayyar, N. West, P. Zhang, C. L. D. McMillan, C. Soemardy, R. Ray, D. O'Meally, T. A. Scott, N. A. J. McMillan and K. V. Morris, *Mol. Ther.*, 2021, **29**, 2219–2226.
2 E. Robinson, K. D. Macdonald, K. Slaughter, M. Mckinney, S. Patel, C. Sun and G. Sahay, *Mol. Ther.*, 2018, **26**, 2034–2046.
3 B. Li, R. S. Manan, S.-Q. Liang, A. Gordon, A. Jiang, A. Varley, G. Gao, R. Langer, W. Xue and D. Anderson, *Nat. Biotechnol.*, 2023, **41**, 1410–1415.
4 A. G. Hamilton, K. L. Swingle and M. J. Mitchell, *PLoS Biol.*, 2023, **21**, e3002105.
5 Q. Cheng, T. Wei, L. Farbiak, L. T. Johnson, S. A. Dilliard and D. J. Siegwart, *Nat. Nanotechnol.*, 2020, **15**, 313–320.
6 M. Qiu, Y. Tang, J. Chen, R. Muriph, Z. Ye, C. Huang, J. Evans, E. P. Henske and Q. Xu, *Proc. Natl. Acad. Sci. U. S. A.*, 2022, **119**, e2116271119.
7 M. Yuan, Z. Han, Y. Liang, Y. Sun, B. He, W. Chen and F. Li, *Biomater. Res.*, 2023, **27**, 90.
8 A. Radmand, M. P. Lokugamage, H. Kim, C. Dobrowolski, R. Zenhausern, D. Loughrey, S. G. Huayamares, M. Z. C. Hatit, H. Ni, A. Del Cid, A. J. Da Silva Sanchez, K. Paunovska, E. Schrader Echeverri, A. Shajii, H. Peck, P. J. Santangelo and J. E. Dahlman, *Nano Lett.*, 2023, **23**, 993–1002.
9 G. Kassab, K. Doran, Y. Mo and G. Zheng, *Nano Lett.*, 2023, **23**, 10099–10102.
10 S. Omo-Lamai, M. E. Zamora, M. N. Patel, J. Wu, J. Nong, Z. Wang, A. Peshkova, L. S. Chase, E.-O. Essien, V. Muzykantov, O. Marcos-Contreras, J. W. Myerson and J. S. Brenner, *bioRxiv*, 2023, preprint, 2023.07.21.550080, DOI: **10.1101/2023.07.21.550080**.
11 M. P. Lokugamage, D. Vanover, J. Beyersdorf, M. Z. C. Hatit, L. Rotolo, E. S. Echeverri, H. E. Peck, H. Ni, J.-K. Yoon, Y. Kim, P. J. Santangelo and J. E. Dahlman, *Nat. Biomed. Eng.*, 2021, **5**, 1059–1068.
12 A. Y. Jiang, J. Witten, I. O. Raji, F. Eweje, C. MacIsaac, S. Meng, F. A. Oladimeji, Y. Hu, R. S. Manan, R. Langer and D. G. Anderson, *Nat. Nanotechnol.*, 2023, 1–12.
13 P. P. H. Le Brun, A. H. de Boer, H. W. Frijlink and H. G. M. Heijerman, *Pharm. World Sci.*, 2000, **22**, 75–81.
14 H. Miao, K. Huang, Y. Li, R. Li, X. Zhou, J. Shi, Z. Tong, Z. Sun and A. Yu, *Int. J. Pharm.*, 2023, **640**, 123050.
15 V. Kumar, J. Qin, Y. Jiang, R. G. Duncan, B. Brigham, S. Fishman, J. K. Nair, A. Akinc, S. A. Barros and P. V. Kasperkovitz, *Mol. Ther.–Nucleic Acids*, 2014, **3**, e210.
16 D. Chen, J. Liu, J. Wu and J. S. Suk, *Expert Opin. Drug Delivery*, 2021, **18**, 595–606.
17 M. Jayaraman, S. M. Ansell, B. L. Mui, Y. K. Tam, J. Chen, X. Du, D. Butler, L. Eltepu, S. Matsuda, J. K. Narayanannair, K. G. Rajeev, I. M. Hafez, A. Akinc, M. A. Maier, M. A. Tracy, P. R. Cullis, T. D. Madden, M. Manoharan and M. J. Hope, *Angew. Chem., Int. Ed.*, 2012, **51**, 8529–8533.
18 World Intellectual Property Organization, WO2017218704A1, 2017.
19 X. Bai, Q. Chen, F. Li, Y. Teng, M. Tang, J. Huang, X. Xu and X.-Q. Zhang, *Nat. Commun.*, 2024, **15**, 6844.
20 X. Murgia, P. Pawelzyk, U. F. Schaefer, C. Wagner, N. Willenbacher and C.-M. Lehr, *Biomacromolecules*, 2016, **17**, 1536–1542.
21 J. Rejman, V. Oberle, I. S. Zuhorn and D. Hoekstra, *Biochem. J.*, 2004, **377**, 159–169.
22 J. A. Kulkarni, M. M. Darjuan, J. E. Mercer, S. Chen, R. van der Meel, J. L. Thewalt, Y. Y. C. Tam and P. R. Cullis, *ACS Nano*, 2018, **12**, 4787–4795.
23 T. Sécher, A. Mayor and N. Heuzé-Vourc'h, *Front. Immunol.*, 2019, **10**, DOI: **10.3389/fimmu.2019.02760**.
24 C. Walsh, K. Ou, N. M. Belliveau, T. J. Leaver, A. W. Wild, J. Huft, P. J. Lin, S. Chen, A. K. Leung, J. B. Lee, C. L. Hansen, R. J. Taylor, E. C. Ramsay and P. R. Cullis, in *Drug Delivery System*, ed. K. K. Jain, Springer New York, New York, NY, 2014, vol. 1141, pp. 109–120.
25 K. V. Kilchrist, S. C. Dimobi, M. A. Jackson, B. C. Evans, T. A. Werfel, E. A. Dailing, S. K. Bedingfield, I. B. Kelly and C. L. Duvall, *ACS Nano*, 2019, 1136–1152.
26 E. N. Donders, K. V. Slaughter, C. Dank, A. N. Ganesh, B. K. Shoichet, M. Lautens and M. S. Shoichet, *Adv. Sci.*, 2023, 2300311.
27 H. Zhang, J. Leal, M. R. Soto, H. D. C. Smyth and D. Ghosh, *Pharmaceutics*, 2020, **12**, 1042.
28 M. T. Neary, L. M. Mulder, P. S. Kowalski, R. MacLoughlin, A. M. Crean and K. B. Ryan, *J. Controlled Release*, 2024, **366**, 812–833.

29 L. Sweeney, A. P. McCloskey, G. Higgins, J. M. Ramsey, S.-A. Cryan and R. MacLoughlin, *Respir. Res.*, 2019, **20**, 66.
30 A. Tam, J. Kulkarni, K. An, L. Li, D. Dorscheid, G. Singhera, P. Bernatchez, G. Reid, K. Chan, D. Witzigmann, P. Cullis, D. Sin and C. Lim, *Eur. J. Pharm. Sci.*, 2022, **176**, 106234.
31 J. Kim, A. Jozic, Y. Lin, Y. Eygeris, E. Bloom, X. Tan, C. Acosta, K. D. MacDonald, K. D. Welsher and G. Sahay, *ACS Nano*, 2022, **16**, 14792–14806.
32 D. Matulis, I. Rouzina and V. A. Bloomfield, *J. Am. Chem. Soc.*, 2002, **124**, 7331–7342.
33 S. Liu, Y. Wen, X. Shan, X. Ma, C. Yang, X. Cheng, Y. Zhao, J. Li, S. Mi, H. Huo, W. Li, Z. Jiang, Y. Li, J. Lin, L. Miao and X. Lu, *Nat. Commun.*, 2024, **15**, 9471.
34 P. Patel, N. M. Ibrahim and K. Cheng, *Trends Pharmacol. Sci.*, 2021, **42**, 448–460.
35 S. Liao, S. Wang, A. Wadhwa, A. Birkenshaw, K. Fox, M. H. Y. Cheng, I. C. Casmil, A. A. Magana, N. V. Bathula, C. H. Ho, J.-Y. Cheng, L. J. Foster, K. W. Harder, C. J. D. Ross, P. R. Cullis and A. K. Blakney, *ACS Appl. Mater. Interfaces*, 2025, **17**, 3097–3105.
36 M. H. Y. Cheng, J. Leung, Y. Zhang, C. Strong, G. Basha, A. Momeni, Y. Chen, E. Jan, A. Abdolahzadeh, X. Wang, J. A. Kulkarni, D. Witzigmann and P. R. Cullis, *Adv. Mater.*, 2023, **35**, 2303370.
37 M. D. I. Manunta, R. J. McAnulty, A. D. Tagalakis, S. E. Bottoms, F. Campbell, H. C. Hailes, A. B. Tabor, G. J. Laurent, C. O'Callaghan and S. L. Hart, *PLoS One*, 2011, **6**, e26768.
38 R. Deshmukh, N. Bandyopadhyay, S. N. Abed, S. Bandopadhyay, Y. Pal and P. K. Deb, in *Drug Delivery Systems*, ed. R. K. Tekade, Academic Press, 2020, pp. 85–129.
39 A. Klemmer, I. Krämer and W. Kamin, *Pulm. Pharmacol. Ther.*, 2014, **28**, 53–59.
40 J. Brillault and F. Tewes, *Pharmaceutics*, 2020, **12**, 387.
41 Q. Gu and L.-Y. Lee, *Curr. Opin. Pharmacol.*, 2011, **11**, 238–247.
42 H. Cortés, H. Hernández-Parra, S. A. Bernal-Chávez, M. L. D. Prado-Audelo, I. H. Caballero-Florán, F. V. Borbolla-Jiménez, M. González-Torres, J. J. Magaña and G. Leyva-Gómez, *Materials*, 2021, **14**, 3197.
43 Y. Seo, H. Lim, H. Park, J. Yu, J. An, H. Y. Yoo and T. Lee, *Pharmaceutics*, 2023, **15**, 772.
44 A. M. Bodratti and P. Alexandridis, *Expert Opin. Drug Delivery*, 2018, **15**, 1085–1104.
45 C. Hogarth, K. Arnold, S. Wright, H. Elkateb, S. Rannard and T. O. McDonald, *Nanoscale Adv.*, 2024, **6**, 669–679.
46 W. C. Griffin, *J. Soc. Cosmet. Chem.*, 1949, **1**, 311–325.
47 F. Lindenberg, F. Sichel, M. Lechevrel, R. Respaud and G. Saint-Lorant, *J. Toxicol. Risk Assess.*, 2019, **5**(1), DOI: **10.23937/2572-4061.1510022**.
48 R. C. Jongejan, J. C. De Jongste, R. C. Raatgeep, I. L. Bonta and K. F. Kerrebijn, *J. Appl. Physiol.*, 1990, **68**(4), 1568–1575.
49 C. Rudolph, R. H. Müller and J. Rosenecker, *J. Gene Med.*, 2002, **4**, 66–74.
50 E. J. Ruijgrok, A. G. Vulto and E. W. M. Van Etten, *J. Antimicrob. Chemother.*, 2001, **48**, 89–95.
51 L. Zhang, K. R. More, A. Ojha, C. B. Jackson, B. D. Quinlan, H. Li, W. He, M. Farzan, N. Pardi and H. Choe, *npj Vaccines*, 2023, **8**, 1–14.
52 N. R. Labiris and M. B. Dolovich, *Br. J. Clin. Pharmacol.*, 2003, **56**, 588–599.
53 B. K. Rubin and R. W. Williams, *Adv. Drug Delivery Rev.*, 2014, **75**, 141–148.
54 A. R. Martin and W. H. Finlay, *Expert Opin. Drug Delivery*, 2015, **12**, 889–900.
55 Y. Ju, C. Cortez-Jugo, J. Chen, T.-Y. Wang, A. J. Mitchell, E. Tsantikos, N. Bertleff-Zieschang, Y.-W. Lin, J. Song, Y. Cheng, S. Mettu, Md. A. Rahim, S. Pan, G. Yun, M. L. Hibbs, L. Y. Yeo, C. E. Hagemeyer and F. Caruso, *Adv. Sci.*, 2020, **7**, 1902650.
56 N. Chander, G. Basha, M. H. Yan Cheng, D. Witzigmann and P. R. Cullis, *Mol. Ther.–Methods Clin. Dev.*, 2023, **30**, 235–245.
57 K. Zhang, J. Hodge, A. Chatterjee, T. S. Moon and K. M. Parker, *Environ. Sci. Technol.*, 2021, **55**, 8045–8053.
58 A. K. Patel, J. C. Kaczmarek, S. Bose, K. J. Kauffman, F. Mir, M. W. Heartlein, F. DeRosa, R. Langer and D. G. Anderson, *Adv. Mater.*, 2019, **31**(8), 1805116.
59 Y. Ju, J. M. Carreño, V. Simon, K. Dawson, F. Krammer and S. J. Kent, *Nat. Rev. Immunol.*, 2023, **23**, 135–136.
60 Y. Ju, W. S. Lee, E. H. Pilkington, H. G. Kelly, S. Li, K. J. Selva, K. M. Wragg, K. Subbarao, T. H. O. Nguyen, L. C. Rowntree, L. F. Allen, K. Bond, D. A. Williamson, N. P. Truong, M. Plebanski, K. Kedzierska, S. Mahanty, A. W. Chung, F. Caruso, A. K. Wheatley, J. A. Juno and S. J. Kent, *ACS Nano*, 2022, **16**, 11769–11780.
61 Y. Xiao, X. Lian, Y. Sun, Y.-C. Sung, A. Vaidya, Z. Chen, A. Gupta, S. Chatterjee, L. Zheng, E. Guerrero, X. Wang, L. Farbiak, Y. Yang, M. I. Diamond, C. Leal, J. G. McDonald and D. J. Siegwart, *Nat. Mater.*, 2025, 1–12.
62 P. Khunsuk, C. Pongma, T. Palaga and V. P. Hoven, *Biomacromolecules*, 2023, **24**, 5654–5665.
63 A. Y. Jiang, S. Lathwal, S. Meng, J. Witten, E. Beyer, P. McMullen, Y. Hu, R. S. Manan, I. Raji, R. Langer and D. G. Anderson, *J. Am. Chem. Soc.*, 2024, **146**, 32567–32574.